Macromolecular Research

Article

DOI 10.1007/s13233-019-7077-5

www.springer.com/13233 pISSN 1598-5032 eISSN 2092-7673

Temperature and Salt-Dependent Dielectric Properties of Blend Solid Polymer Electrolyte Complexed with LiBOB

Anil Arya
Achchhe Lal Sharma*

Department of Physical Sciences, Central University of Punjab, Bathinda, India

Received May 11, 2018 / Revised October 17, 2018 / Accepted November 9, 2018

Abstract: In the present paper, the temperature and salt-dependent dielectric properties of poly(ethylene oxide) (PEO) and poly(vinyl pyrrolidone) (PVP) blend matrix complexed with LiBOB are investigated in the frequency range 1 Hz to 1 MHz and temperature range 40 °C to 100 °C (@10 °C). The real and imaginary part of the complex permittivity, complex conductivity have been simulated in the whole frequency window and the various fitted parameters were evaluated respectively. The estimated value of the dielectric constant and the ac conductivity increases with the increase of temperature. The lowering of relaxation time and hopping length is observed with the salt addition that is in correlation with the complex conductivity results. The modulus formalism was used to analyze the recorded dielectric data. The dc conductivity, hopping frequency, and segmental motion are strongly coupled with each other as evidenced by the Debye-Stoke-Einstein (DSE) plot. An interaction mechanism has also been proposed to explore the effect of temperature on the hopping length, relaxation time, hopping potential barrier and the segmental motion of the polymer chain.

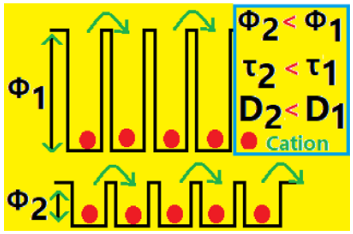

Keywords: blend solid polymer electrolyte, complex permittivity, relaxation time, ion transport mechanism.

1. Introduction

Due to increasing demand of energy and depletion of the traditional energy resources such as coal, fossil fuels *etc*; it becomes crucial to develop alternate/renewable resources of energy such as solar energy, wind energy, and ocean energy. The most promising energy storage system is the Li-ion battery (LIB) due to various advantages associated, such as high energy density, better cyclic stability and is mostly fulfilling the need of energy source in portable electronics.[1-4] A typical battery comprises of three components cathode, anode, and electrolyte. The electrolyte is sandwiched between the electrodes and it permits the shuttling of ions in-between electrodes. Therefore, the electrolyte must be compatible with both electrodes for the operation of the battery. Polymer electrolytes are attractive candidates due to associated advantages; easy availability, shape integrity and ease of fabrication which the commercial electrolyte lacks. Although gel polymer electrolyte possesses improved properties as compared to liquid electrolyte but, poor mechanical properties prevents its use. To overcome the above-said issues, solid polymer electrolyte (SPE) are promising candidates and can replace the gel polymer electrolyte and traditional liquid electrolytes.[5-10] Solid polymer electrolytes have various advantages, such as flexibility, shape integrity, reduced weight, good interfacial contact, leak-proof, and operational safety. The ion migration in such systems is supposed to be through the amorphous phase of the polymer matrix *via* ion hopping and the segmental motion of the polymer chain. The chain reorganization plays an effective role in the ion migration *via* segmental motion and promotes the ion migration that enhances the ionic conductivity.[11-15]

The most investigated host polymer is the poly(ethylene oxide) (PEO) due to its broad range of complex formation with salts and presence of electron rich ether group facilities the salt dissociation *via* cation---ether group (-O-) interaction.[16,17] But, it possesses poor ionic conductivity, which limits its use for practical applications. So, various strategies, blending, crosslinking and grafting have been adopted to enhance the ion migration. Out of these blending approach is most promising as it facilitates the easy preparation and cost-effective.[18,19] The polymer blends are prepared by the physical mixing of the two or more polymers and provide improved properties which an individual polymer lacks.[20-23] Recently, many efforts have been devoted toward the enhancement of the electrochemical and mechanical properties in blend solid polymer electrolyte membranes such as PEO-PAN, PVdF-PEO, PEO-P(VdF-HFP), PVA-PEO, PEO-PEG, PVA-PVP, PVC-PVdF, PEO-PVP, and PVC-PEO.[24-31]

The PVP has been chosen to prepare blend polymer electrolyte due to high amorphous content and better thermal/environmental stability. The interaction between the blend polymer electrolyte and the salt disrupts the crystalline arrangement and facilitates the smoother ion migration.[32-35] The salt Lithium bis (oxalato)borate (LiBOB; $LiBC_4O_8$) has been chosen due to advantages; bulky anion size, low cost, high thermal stability, and environment-friendliness. The bulky anion size leads to poor anion and faster cation mobility. Numerous reports have been published using the LiBOB as salt with different polymers PVdF, PVA, PEO but may improve the performance after using the blend instead of the individual host polymer.[36-40]

The ion migration in the solid polymer electrolyte is *via* the hopping process. In the polymer matrix, the creation and destruc-

Acknowledgments: One of the author AA is thankful to the Central University of Punjab for providing fellowship.

***Corresponding Author:** Achchhe Lal Sharma (alsharma@cup.edu.in)

tion of coordinating sites occur that supports the ion migration from one site to other and ion hopping depends on the relaxation process of the polymer chains. The relaxation time is generally the time taken in between the end of hopping and start of another ion for hopping. In, brief it may be stated that the segmental motion of the polymer chain affects the ion migration and hence the ion mobility. Ion transport mechanism is also important to elaborate and to get the insights of ion dynamics. The impedance spectroscopy is the best tool to investigate the ion dynamics in terms of dielectric properties. Therefore, impedance data is transformed into the dielectric parameters such as dielectric constant, dielectric loss, loss tangent, ac conductivity, and modulus.[41-44]

In the present paper, we studied the effect of salt concentration and temperature on the ion dynamics and dielectric relaxation of PEO-PVP based solid polymer electrolyte complexed with LiBOB, prepared by the solution cast technique. The complex permittivity, loss tangent, complex conductivity, and modulus formalism were evaluated and analyzed systematically. Finally, an ion transport mechanism was proposed to highlight the role of salt content and temperature on the prepared blended solid polymeric electrolyte system.

2. Experimental

2.1. Materials

The polymer host PEO (av. Mol. Wt.; 200,000, Sigma), blend polymer PVP (av. Mol. Wt.; 40000, Sigma), LiBOB (Mol. Wt. 167.95 g/mol, Sigma) and methanol (Loba) were used as received. An appropriate amount of the polymer (80:20) and salt (O/Li^+=16, 18, 20, 22, 24) were mixed methodically using the common solvent methanol by standard solution cast technique. First of all PEO and PVP were added in methanol (20 mL) and kept for 10 min for swelling of polymer chains followed by 4 h stirring. Then the appropriate stoichiometric ratio of salt (O/Li^+=16, 18, 20, 22, 24) were added to the homogeneous solution and stirred for 12 h before casting in the Petri-dishes. Then after drying at room temperature first and then in a vacuum oven (for 24 h), the prepared film is peeled off from Petri-dishes and stored in a desiccator to avoid any contamination and moisture free solid polymeric films.

2.2. An overview of dielectric properties

Dielectric properties of the synthesized BSPEs are investigated in terms of the Cole-Cole plot, Complex dielectric permittivity, loss tangent plot, Complex conductivity, and the modulus formalism. Then the various dielectric parameters such as dielectric constant, dielectric loss, relaxation time, modulus relaxation time, hopping frequency and ac conductivity are evaluated. We have also simulated the Complex permittivity, loss tangent and complex conductivity plot in the whole frequency window to get proper insight of the dielectric relaxation and its influence on the ion dynamics in the blend polymer matrix. Various fitting parameters such as dc conductivity, relaxation time and bulk capacitance are evaluated.

The complex dielectric permittivity has two parts, real part (ε') describes the storage capacity or dielectric constant while the imaginary part (ε'') is the dielectric loss expressed as $\varepsilon^*=\varepsilon'-j\varepsilon''$. The real and imaginary parts of complex permittivity were used to fit the real and imaginary part of complex permittivity reported in our previous published article.[46,47] Now, another significant parameter is the loss tangent and modified Debye equation ($\tan\delta=\left(\frac{(r-1)}{r+x^2}x\right)^{\alpha}$ is used to fit the loss tangent plot.[46] It is interesting to observe here that the modified equation simulate the loss tangent plot in the whole frequency window, in contrast to ideal Debye equation which is not reliable at the low frequency window.

The frequency dependent complex conductivity comprises of the real and imaginary part of the conductivity is expressed as, $\sigma(\omega)=\sigma'(\omega)+i\sigma''(\omega)$.[48,49] Another interesting formalism is modulus formalism that provides insight of ion dynamics by suppressing the electrode polarization. The general relation comprise of modulus is in inverse relation with complex dielectric permittivity, real & imaginary part are expressed as, $M^*=1/\varepsilon^*=M'+jM''=\{\varepsilon'/(\varepsilon'^2+\varepsilon''^2)\}+i\{\varepsilon''/(\varepsilon'^2+\varepsilon''^2)\}$.[50] The samples are labeled as PP, PP16, PP18, PP20, PP22, and PP24 for blend solid polymer electrolyte films with O/Li^+=16, 18, 20, 22, 24 of LiBOB respectively, for further investigation.

3. Results and discussion

3.1. Complex permittivity analysis

Dielectric properties of the blend solid polymer electrolyte are studied in terms of the Cole-Cole plot, complex dielectric permittivity, loss tangent, complex conductivity, and modulus formalism. Various vital parameters such as dielectric constant, dielectric strength, double layer capacitance, relaxation time, hopping frequency and ac conductivity are evaluated from the fitting of the complex dielectric permittivity, loss tangent and complex conductivity plot in the whole frequency window.[51]

3.1.1. Cole-Cole analysis

The Cole-Cole plot (ε'' *vs.* ε') depicts the dielectric loss plotted against the dielectric constant with frequency as variable parameter.[47,52] The Cole-Cole plot is analyzed from right to left with an increase of frequency (Figure 1) at room temperature. The semicircular arc in all the BSPEs system is attributed to the spread of relaxation time. The maxima in the extrapolated semicircle is observed at the mid-point and the presence of the spike evidences the heterogeneous relaxation process. The solid red line depicts the fitted plot of the Cole-Cole plot and the intersection on the *x*-axis gives the ε_∞ (dielectric constant at an infinite frequency) and ε_s (static dielectric constant). For both parameters (ε_∞ & ε_s) the dielectric loss tends to zero.[53] It can be noticed from the Figure 1 that the increase in the dielectric constant value implies the increase in number of free charge carriers and hence more ions are stored.[54] This will be further explored in the complex dielectric permittivity analysis.

3.1.2. Real and imaginary part of the complex permittivity analysis

Figure 2(a), (b) illustrate the frequency dependent complex dielec-

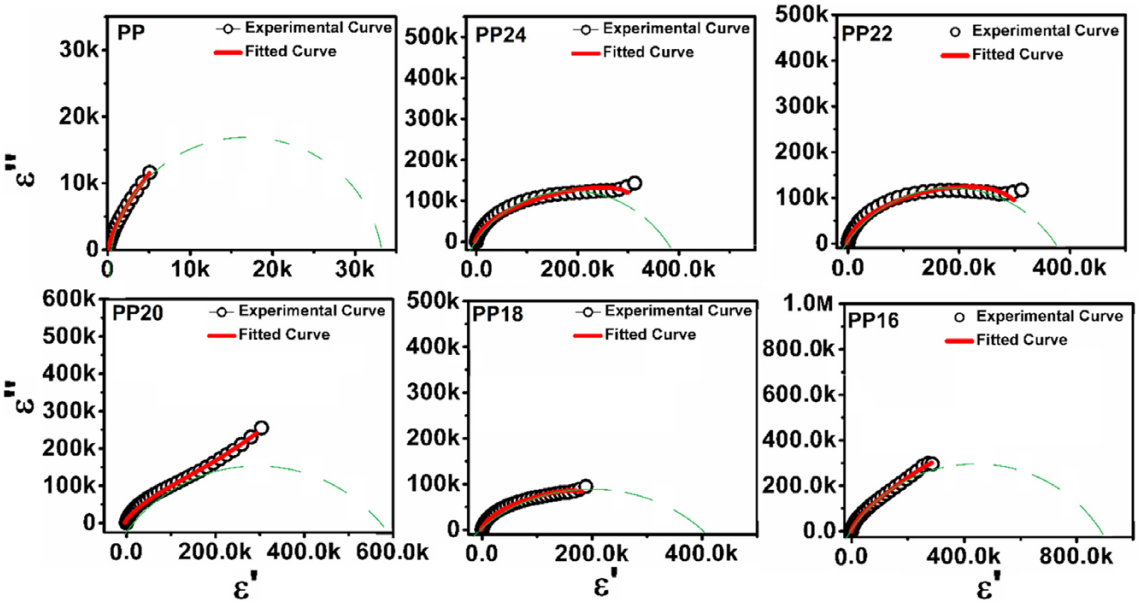

Figure 1. Cole-Cole plot of the blend solid polymer electrolyte films.

tric permittivity for blend polymer electrolyte complexed with different salt content. The complex dielectric permittivity has two parts, real part (ε') describes the storage capacity or dielectric constant while the imaginary part (ε'') is the dielectric loss. All the plots exhibit the identical trend of decrease of the dielectric permittivity and dielectric loss with an increase of the frequency. It is observed in Figure 2(a), that in low-frequency window the high value of the dielectric constant is observed and is attributed to dominance of the space charge (atomic/electronic) electrode polarization at electrode/electrolyte interface. The two types of dipoles, free ions due to salt dissociation and polar polymer groups are two factors that lead to a high dielectric constant at low frequency.[55]

Now, in the high-frequency region dielectric constant/orientational polarization decreases due to the hindrance of long-range ion migration and becomes constant at a later time. This steady-state dielectric constant is termed as ε_∞ and in this region orientation polarization ceases and ion migration is frozen.[43,56] The decrease of the dielectric constant is attributed to the lag between the frequency of the applied field and ion dipoles. Now ion dipoles are unable to respond quickly to the applied electric field in sufficient time. In this region, the ion-ion interaction decreases in transient dipoles (cation---ether group). So, the overall ion migration will be only due to the long-range ion charge carriers.[57-60] Now, the addition of salt in the blend polymer matrix further increase the dielectric constant, dielectric strength ($\Delta\varepsilon$) and may be attributed to the increased number density of free charge carriers owing to the better salt dissociation.[61] In polymer electrolytes, the number of charge carriers depends on the dissociation energy and the dielectric constant by equation $n=n_o \exp\left(-\frac{U}{\varepsilon' kT}\right)$.[54]

The above equation indicates the increase in the number of charge carriers. As dielectric constant depicts the storage capacity of ions and high value of dielectric constant imitates the additional number of ions stored. This is consistent with the increase in salt concentration and increased polymer flexibility. Here, the segmental motion of the polymer chain also plays an effective role and growth of additional charge polarization takes place due to contribution from dipole orientation and better salt dissociation.[29]

In Figure 2(a), change of slope in the mid-frequency window indicates the presence of segmental relaxation. While with the

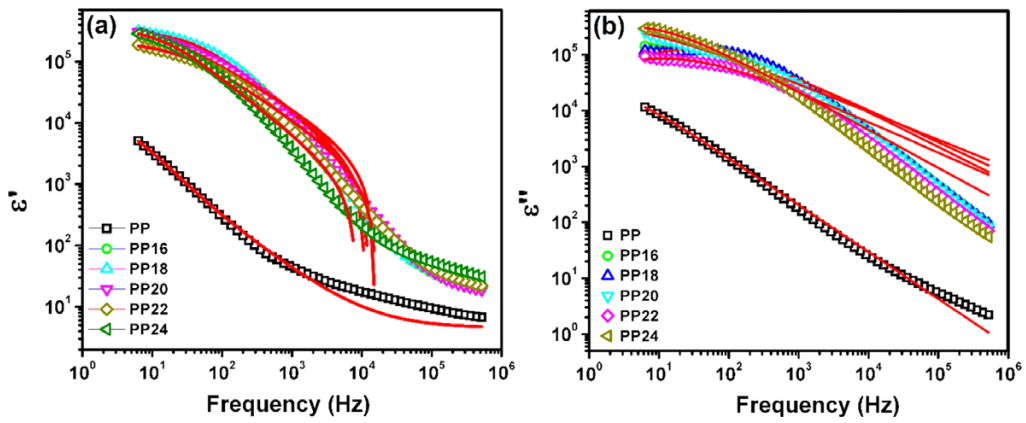

Figure 2. The plot of (a) real part of complex permittivity and (b) imaginary part of complex permittivity against the frequency.

addition of salt ionic conductivity is increased and it masks the segmental relaxation process distinguishable in Figure 2(b).[62] Beside dielectric permittivity, dielectric loss is also associated with the blend polymer electrolyte. Initially, when the field is applied then the ion migrates along field direction and on the reversal of field all dipoles are unable to respond and half the ion diffusion occurs in the field direction. This results in the heat generation in dielectric and is termed as dielectric energy loss (ε''=0 for $\omega\tau$=0). The dielectric loss at low frequencies is mainly due to dc resistivity while at high frequencies is due to dipole rotations from low to high energy states.[63]

The real and imaginary parts of complex permittivity are fitted in the whole frequency window. The solid red lines in the plot are best fit to the corresponding equation and fitted parameters are summarized in Table 1. From the Figure 2 it can be observed that both the real and imaginary part of the complex permittivity displays good agreement at the low frequency where electrode polarization is effective while some deviation at the high frequency is observed. It may be due to the dominance of the frequency dependent segmental relaxation mechanism and may be explained by the Harvriliak and Negami (HN) equations.[49,62] It is observed in Table 1 that the dielectric strength increase with the addition of the salt. The absence of relaxation peak in all graphs may be due to large electrode polarization effect which masks the relaxation behavior of polymer electrolytes. Therefore, electric modulus and ac conductivity are attempted as alternatives to study ion dynamics in the next sections.

3.2. Loss tangent analysis

The loss tangent plot consists of a single peak and indicates that the ion conduction is *via* the polymer segmental motion. Figure 3 displays the variation of the loss tangent ($\tan\delta=\varepsilon''/\varepsilon'$) plot against the frequency of different salt content. The process of loss tangent is correlated with the ion mobility and the ionic conductivity. The area under the loss tangent plot reflects the number of ions contributing to the relaxation process.[58] Figure 3

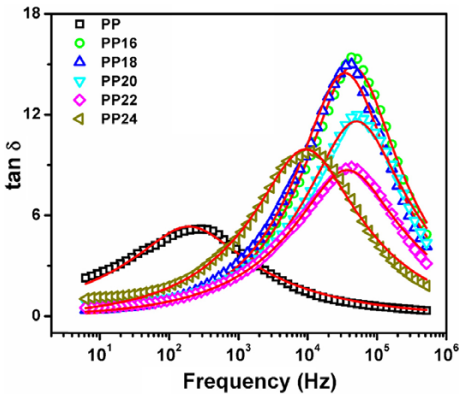

Figure 3. Frequency dependence of the tangent delta loss (tan δ) for blend polymer electrolyte.

shows the variation of the loss tangent plot of blend polymer electrolyte with different salt content. All the plots exhibit the same trend with a peak at a particular frequency. The plot is divided into three regions, in lower frequency region increase of loss tangent is attributed to the dominance of Ohmic component over the capacitive component, While, at high-frequency decrease is attributed to the independent nature of Ohmic part and growing nature of reactive component. The peak in the plot is associated with the maximum transfer of energy for the particular frequency ($\omega\tau\approx1$) on the application of filed.[64,65] The relaxation peak shifts toward the high frequency window on the addition of salt and it indicates the decrease of relaxation time, and hence the fast segmental relaxation. The addition of salt content evidences the increase of the amorphous content and lowering of relaxation time is confirmed by the shift of peak toward high frequency.[58] The decrease of the relaxation time suggests the speed up of the ion migration from one coordinating site to other.

So, all the loss tangent plots were fitted with the associated equation and the fitted parameters are given in Table 2. A previous report displays an inability to fit at low frequency.[66] The

Table 1. The fitted ε' (ε_∞, $\Delta\varepsilon$, $\tau_{\varepsilon'}$, α) and ε'' ($\Delta\varepsilon$, $\tau_{\varepsilon''}$, α) parameters at room temperature

Sample code	ε'				ε''		
	ε_∞	$\Delta\varepsilon$	$\tau_{\varepsilon'}$ (s)	α	$\Delta\varepsilon$	$\tau_{\varepsilon''}$ (s)	α
PP	6	14953	2.84×10^{-6}	0.82	47324	2.11×10^{-6}	0.83
PP16	19	34861	1.03×10^{-8}	0.71	542053	1.73×10^{-8}	0.58
PP18	24	337041	9.28×10^{-9}	0.74	461458	1.22×10^{-8}	0.62
PP20	19	427308	2.14×10^{-9}	0.62	1548000	1.27×10^{-7}	0.50
PP22	22	225489	2.10×10^{-8}	0.66	368447	3.96×10^{-8}	0.52
PP24	30	381576	2.36×10^{-8}	0.74	1041400	3.72×10^{-8}	0.68

Table 2. The fitted tangent delta loss parameters (r, τ, α, $\tau_{tan\,\delta}$, τ_m) at room temperature

Sample Code	r	τ	α	$\tau_{tan\,\delta}$ (s)	τ_m (s)
PP	33300	0.938	0.37	5.14×10^{-3}	2.81×10^{-5}
PP16	720.75	0.006	0.55	2.26×10^{-5}	8.43×10^{-8}
PP18	65891	0.007	0.55	2.89×10^{-5}	1.12×10^{-7}
PP20	106795	0.006	0.48	1.98×10^{-5}	6.06×10^{-8}
PP22	75364	0.007	0.43	2.68×10^{-5}	9.79×10^{-8}
PP24	93638	0.032	0.45	1.06×10^{-4}	3.48×10^{-7}

fitted plot is in good agreement with the experimental data points in the whole frequency window and issue of deviation in the low-frequency window is resolved.

The loss tangent plot is in good agreement with the fitted results as indicated by the solid red line. In the low-frequency, the negligible deviation is visible in blend polymer matrix with salt and may be due to the electrode polarization or diffusion of ions towards the electrodes.[67] As the area under the loss tangent curve expresses the number of ions participating in the relaxation process. The area under the curve is highest for the polymer electrolyte with the highest ionic conductivity.

3.3. Real and imaginary part of the complex conductivity analysis

Figure 4(a), (b) shows the variation of real and imaginary part of the conductivity against the frequency for blend polymer electrolyte with different salt content. It is noticed from the plot that all plot comprises of three regions classified on the basis of frequency, low-frequency electrode polarization region, frequency independent dc conductivity region and, high-frequency dispersive region (indicated by dotted line in Figure 4(a).[49] The electrode polarization (EP) phenomena dominate in the low-frequency region and it lowers the ac conductivity value. The EP region disappears with an increase of frequency as we move from left to right in the plot. Then the frequency independent region is observed which designates the dc conductivity value associated with the long-range ion migration *via* coordinating sites provided by the polymer matrix. Now, the most striking region is the dispersive region in the high-frequency zone that is linked with the hopping of charge carriers having a short range of ion transport. The ac conductivity in this region is because of two phenomena's, one is long-range ion conduction (associated with migration of ions) and hopping conduction mechanism (*via* polymer hetro-sites).[57,68] The switch from the dc conductivity region to power-law formalism in the high-frequency window indicates the relaxation phenomena and long-range migration of charge carriers. It is also observed that the EP window increases with the addition of the salt and high-frequency dispersive region also shifts toward high frequency. It suggests that both electrode polarization region and the dispersive region exhibit mutual correlation. The jump relaxation model explains the relaxation.[69-71] This model states that at low-frequency ion migration occurs *via* jumps from one site to another, from where dc conductivity is extracted, while at high-frequency relaxation is the result of simultaneous contribution from forward-backward hopping & ion relaxation.[72]

The frequency dependent imaginary part of the conductivity (σ'') is shown in Figure 4(b). It is observed that the σ'' of polymer electrolyte system also comprises of three regions, low frequency dispersion (electrode polarization) region, and intermediate frequency independent region followed by the high frequency dispersion region. When we move from right to left (towards low frequency) in the plot σ'' decreases rapidly. The low frequency EP region (at electrode/electrolyte interface) starts to dominate at a particular frequency ω_{on} and a minima in σ'' is noticeable. With, further lowering of the frequency increase in the σ'' is demonstrated and electrode polarization phenomena is more effective. Then at particular frequency maximum polarization is achieved termed as ω_{max} and peak in the σ'' is visible. Also, at this frequency reduction in the σ' starts when we move from high to low frequency. Further, with decrease of the frequency a peak in σ'' starts to grow up and maxima in the σ'' is evidenced. Further with decrease of frequency, a decrease in the conductivity is observed.[73,74] The dotted line in the plot divides the plot in three regions and both ω_{max} and ω_{on} shift toward high frequency side while electrode polarization (EP) get broadened with addition of salt. The addition of salt in the blend polymer electrolyte increase the dc conductivity and dispersive region disappears as displayed in the Figure 4(a). This concludes that the electrode polarization region and dispersive region are mutually correlated.

We also simulated the real and imaginary part of the complex conductivity experimental data by the equations proposed by Roy *et al.*,[49] It is interesting to notice here that both the real and imaginary part of the electrical conductivity are in absolute agreement with the experimental data points in whole frequency window (solid red line). The fitted plot of the real and imaginary part of conductivity shows perfect agreement with the experimental results and fitted parameters such as dc conductivity, double layer capacitance, hopping frequency, bulk capacitance, and fractional exponent n & s are summarized in Table 3. It is also noted that the value of the exponential parameter is less than unity. The conductivity value obtained from the impedance study shows maxima for the sample PP16 while the dc conduc-

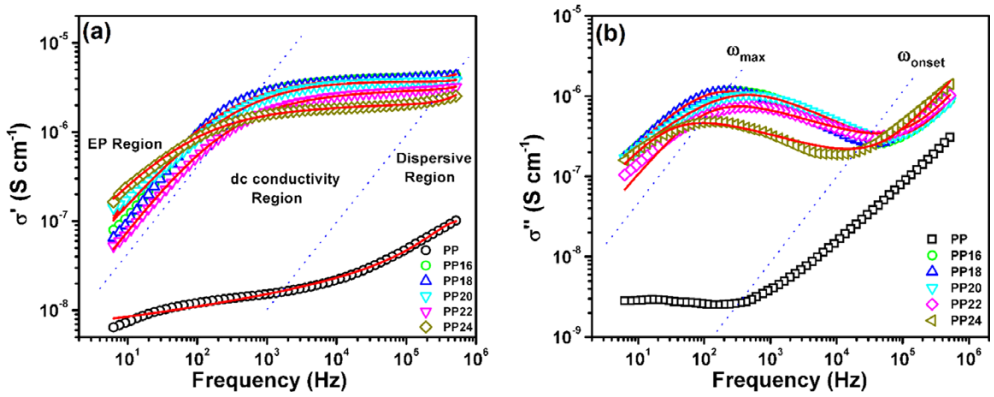

Figure 4. (a) Frequency dependence of real part of complex conductivity (σ'). (b) Frequency dependence of Imaginary part of complex conductivity (σ'') at RT with different salt concentration. Solid lines are absolute fit.

Table 3. Comparison of fitted parameters for real and imaginary part of the complex conductivity

Sample Code	Real part of complex conductivity (σ')					Imaginary part of complex conductivity (σ'')				
	σ_b (S cm^{-1})	ω_h	α	n	C_{dl} (F)	A (S cm^{-1})	s	C_{dl} (F)	α	C_{dl} (pF)
PP	4.60×10^{-9}	17.45	0.19	0.43	1.46×10^{-5}	2.02×10^{-5}	0.43	5.52×10^{-8}	0.72	1.67
PP16	1.81×10^{-5}	248.25	0.98	0.49	6.07×10^{-7}	1.01×10^{-5}	0.41	4.19×10^{-8}	0.81	1.97
PP18	1.80×10^{-5}	216.34	0.99	0.48	6.69×10^{-7}	2.92×10^{-5}	0.41	6.74×10^{-8}	0.62	1.53
PP20	8.59×10^{-5}	308.43	0.93	0.46	7.42×10^{-7}	1.46×10^{-7}	0.25	1.14×10^{-8}	0.98	1.72
PP22	1.17×10^{-5}	252.76	0.92	0.52	3.05×10^{-7}	1.03×10^{-7}	0.23	2.73×10^{-8}	0.97	2.80
PP24	2.16×10^{-5}	67.39	0.85	0.43	1.03×10^{-6}	1.03×10^{-7}	0.23	2.73×10^{-8}	0.97	2.80

tivity value obtained from the fitted plot show maxima for PP20. Generally, in the impedance study, a constant electric field is applied and the corresponding conductivity is obtained. But, now since the electrode polarization region is also included in the fitting so both values do not coincide.

3.4. Modulus Study

Modulus formalism is an effective approach to understand the ion transport with frequency, as it supports the understanding of relaxation mechanism by suppressing the low-frequency electrode polarization. For investigating the modulus formalism, the impedance data is transformed into the modulus data. Figure 5(a), (b) displays the plot of real and imaginary part of modulus as a function of frequency for different salt concentration. Both the plots exhibit the same trend and at high-frequency dispersion is observed. The low value of M' in low frequency window evidences masking of the electrode polarization. The tail at lower frequency window get lengthens with the addition of salt and evidences the large capacitance associated in present system. The dispersion region suggests that the long range of ion migration dominates due to less restoring force on the application of filed.[29,58,75-77]

The imaginary modulus also shows relaxation peak at high frequency for blend polymer electrolyte without salt. This part is linked to the migration of the ions *via* hopping mechanism

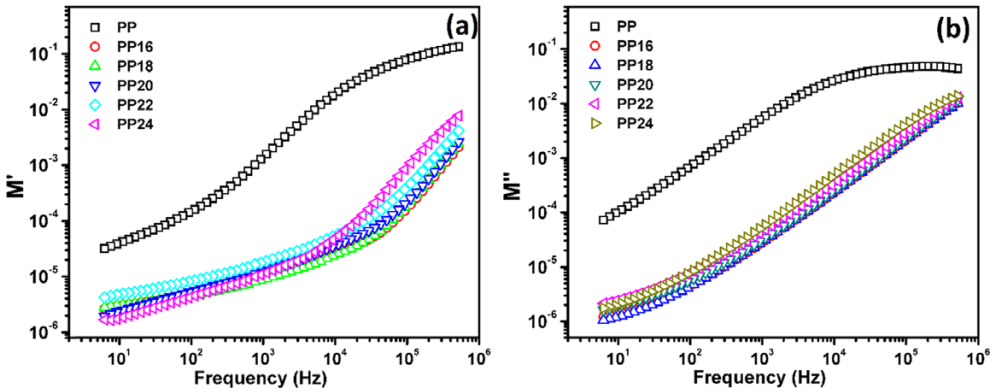

Figure 5. Frequency-dependent (a) real (M') and (b) imaginary part (M'') of modulus spectra.

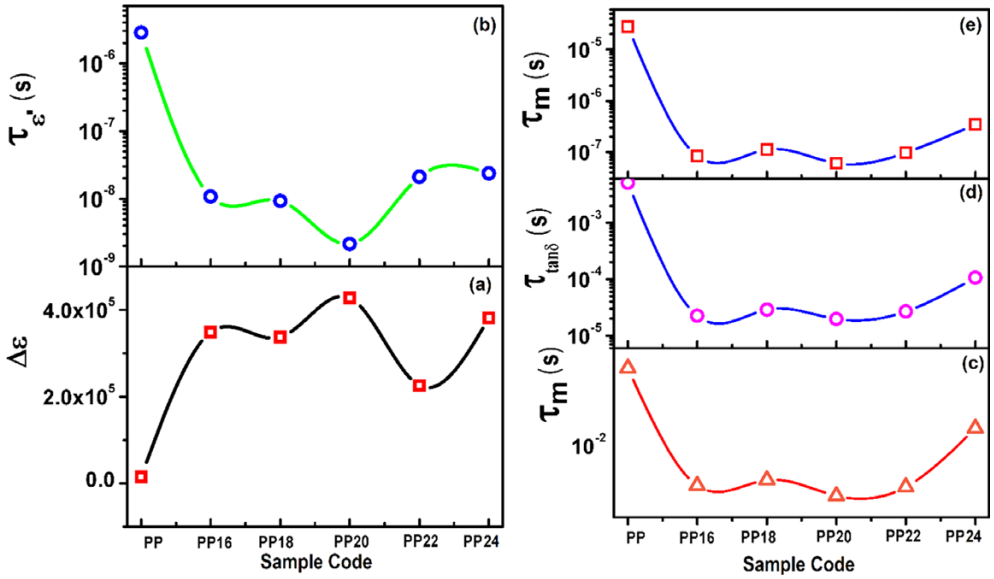

Figure 6. The plot of (a) dielectric strength and (b-e) relaxation time with different salt content in the blend polymer matrix.

from one coordinating site to the other. The right side of the peak indicates confined mobile carriers to potential wells and left of the peak indicates long-range ion migration. The peak frequency depicts the relaxation frequency at which long-range ion motion switch to short range ion motion with an increase of frequency.[25,78-79] While with the addition of salt peak falls outside the measured frequency window (1 Hz-1 MHz) and evidences the lowering of relaxation time. The low value of relaxation time is linked with faster ion migration and is desirable for a solid state ionic conductor.[44,80,81] The modulus relaxation time (τ_m) was calculated in the earlier section using the loss tangent simulation parameter's and illustrates the decrease of relaxation time with the addition of the salt (Table 3). Figure 6 shows the variation of the dielectric strength and the relaxation time against the salt concentration of the blend polymer electrolyte system. It is interpreted that the addition of salt increases the dielectric strength that is attributed to the better salt dissociation *via* polymer-salt interaction. So, more free ions are available for the polarization which enhances the dielectric strength. From the fitting of the appropriate equations, various relaxation times are obtained. It is observed that the addition of the salt lowers the relaxation time that indicates faster ion migration. The lowering of the relaxation time may be due to the enhanced amorphous content and altered polymer chain arrangement owing to the interaction of the electron-rich group and cation. All the relaxation time shows the same trend with salt content.

3.5. Temperature dependent dielectric properties

3.5.1. Complex permittivity analysis

The complex permittivity analysis was performed in the frequency range from 1 Hz to 1 MHz and in the temperature range 40 °C-100 °C @10 °C. The complex permittivity analysis enables us to evaluate the dielectric properties dependent on the frequency as well as temperature. Two important points which are studied is the capacitive nature and conductive nature. The former one tells about the storage ability of the material while the latter indicates the ability of dielectric to transfer the charge of the material.[82] The large value of dielectric constant or dielectric strength enables us to store the more energy, as $U_e \propto \varepsilon_r$.[83]

3.5.2. Real part of complex permittivity

It is observed from the Figure 7(a)-(e), that the dielectric permittivity continuously decreases with the increase of the frequency in all systems irrespective of temperature. The increase in low frequency is due to the electrode polarization owing to the quick response of dipoles to the applied electric field which leads to charge accumulation at electrodes due to blocking stainless-steel (SS) electrodes. The decrease in high frequency is due to the inability of ions to respond to the applied field or decrease of orientation polarization and hindrance of ion diffusion due to the rapid changing of the field. This lowers the ion contributions to the dielectric constant and evidences the Non-Debye nature (ω^{n-1}) in present system.[29,84] At low frequency, all polarization built up to contribute to the enhancement of dielectric constant but during the transition from low to high-frequency polarization having large relaxation time ceases with the application of field and decreases dielectric constant.[85] It need to be mention here that the drop in the dielectric constant is not rapid as delay in polarization seems to be observed on application of the field due to inertia which lowers the dielectric constant.[64] Figure 7 displays the temperature dependent dielectric permittivity for various solid polymer electrolyte system. The increase in the temperature increases the dielectric constant at every frequency due to the polar nature of the polymer blend.[86] The increase of the temperature makes dipole rotation easy

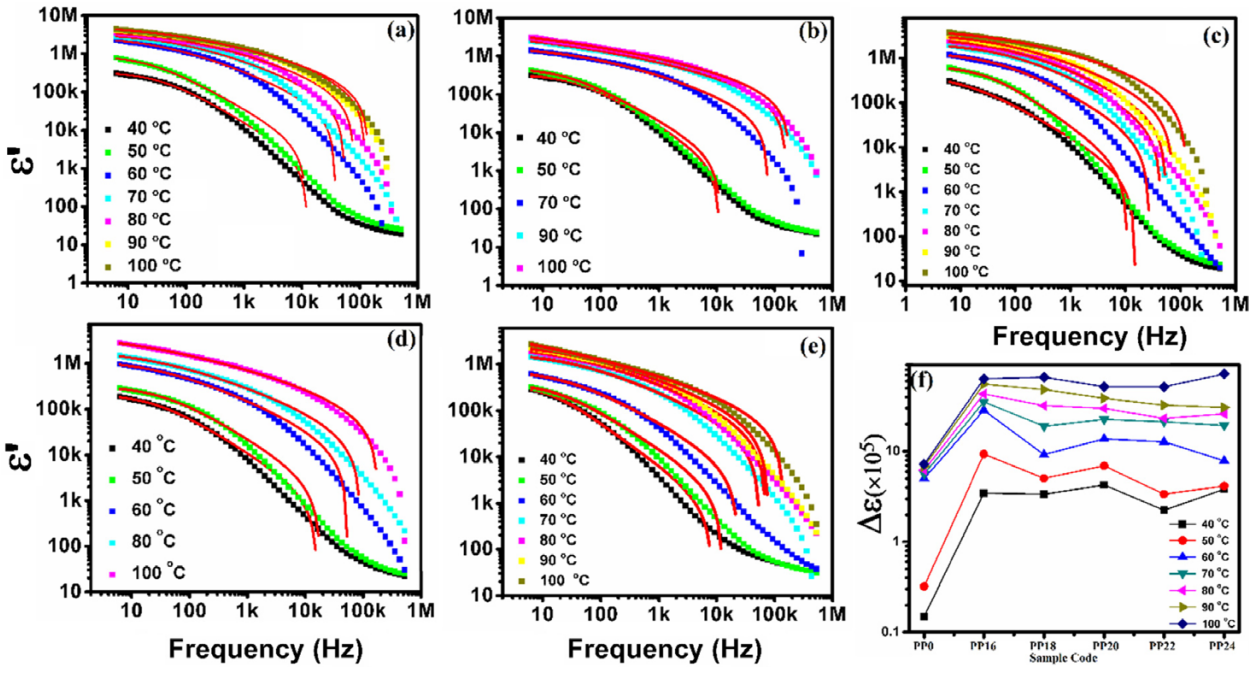

Figure 7. Frequency dependence of real part of complex permittivity (ε') for (a) PP16, (b) PP18, (c) PP20, (d) PP22, (e) PP24 and (f) variation of dielectric strength ($\Delta\varepsilon$) with temperature.

and this leads to the enhancement of the dielectric permittivity. The change in slope of the plot at low frequency with an increase of temperature and indicates the contribution *via* segmental motion of the polymer chain in ion transport.[62]

Another reason for the enhancement of the dielectric permittivity is the faster segmental motion of polymer chain which also supports the enhancement of the electrode polarization. The increase of temperature also supports the dissociation of the salt and hence the dielectric constant. The salt dissociation is linked with the lowering of the activation energy ($E_a=q^2/4\pi\varepsilon_o\varepsilon_s r$).[87] The electrode polarization is the result of quick dipole orientation on the application field as temperature internally activates the dipoles to respond with the applied field. The dispersion regions also shift towards high frequency with an increase of temperature and indicates the reduction of relaxation time. The lowering of relaxation time is linked with the enhanced electrical conductivity and hence the dielectric constant. The same behavior is observed for all the solid polymer electrolyte systems.

The solid lines in the Figure 7(a)-(e) fit well to the experimental results while at high frequency is not well fitted. Figure 7(f) shows the variation of the dielectric strength ($\Delta\varepsilon=\varepsilon_s-\varepsilon_\infty$) for various solid polymer electrolyte at different temperature. It concludes that the dielectric strength increases with the temperature for all systems and is attributed to the enhancement of number of free charge carriers which enhances the electrode polarization at the electrode-electrolyte interface.

3.5.3. Imaginary part of complex permittivity

Figure 8(a)-(e) shows the plot of the imaginary part of the complex permittivity (dielectric loss) with frequency and temperature variation for different solid polymer electrolyte system. The dielectric loss decreases with the increase of frequency and rises with lowering of frequency. The rise in the dielectric loss at low frequency is attributed to the dominance of electrode polarization and space charge polarization at the electrode-electrolyte interface which is the signature of non-Debye type nature.[88]

In all the systems, the dielectric loss increase with the increase of the temperature and no peak corresponding to maxima in dielectric loss is observed. So, to obtain the peak in solid electrolytes the dc conductivity is separated from the total conductivity but in case of ion conducting systems the presence of electrode polarization results in large experimental error so such situation is avoided.[72,89] All the investigated system follows the same trend and the peak (shown by the dotted circle) shift toward high frequency with an increase of the temperature. Figure 8(f) shows the variation of relaxation time and the conductivity with the temperature. It is observed that the relaxation time decrease with the increase of temperature and conductivity increases. This nature is evidence of the increase in the segmental motion of the polymer chain and enhanced flexibility. With the increase of the temperature, the cation gets thermally activated and migrates at a faster rate *via* the coordinating sites in the blend polymer matrix. This evidences that on increase of temperature free volume available for the ion migration increases.

3.6. Complex conductivity analysis

The complex conductivity is expressed as $\sigma'=\sigma'+i\sigma''$; where σ' is real part of complex permittivity, and σ'' is imaginary part of the complex permittivity. The detailed analysis of the temperature dependent real and imaginary part is as follows.

3.6.1. Real part of complex conductivity

Figure 9(a)-(e) shows the frequency and temperature dependent ac conductivity for different solid polymer electrolyte system. All investigated systems show the increase of conductivity with the frequency and temperature. The plot may be divided into three regions independent of temperature, (i) sharp increase

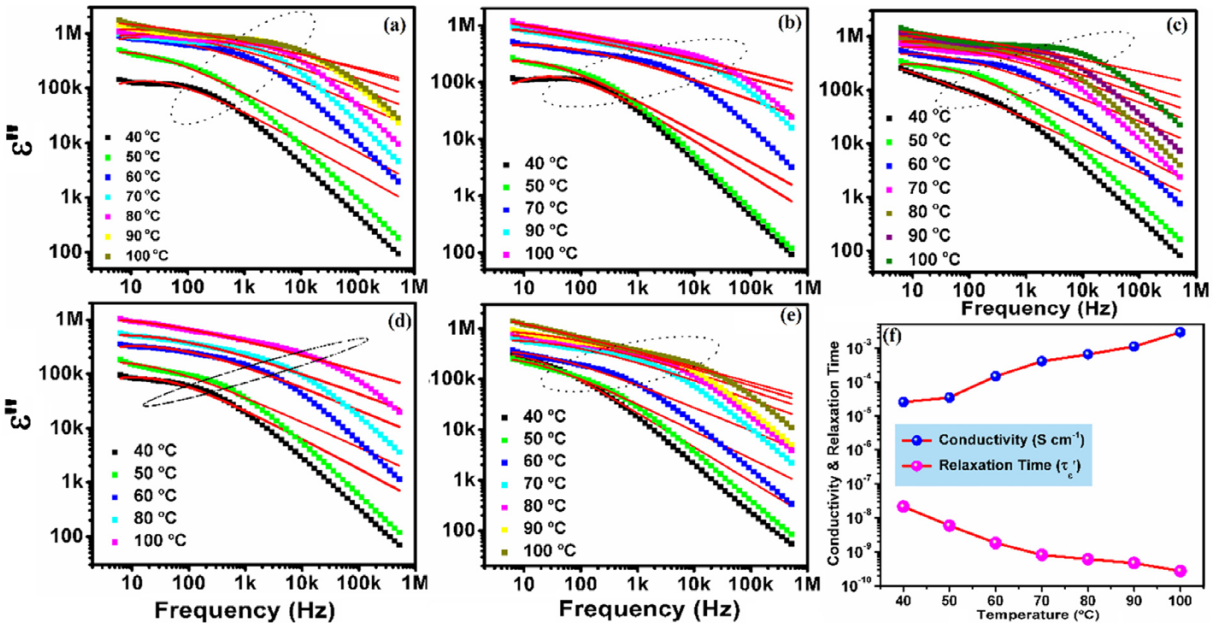

Figure 8. Frequency dependence of imaginary part of complex permittivity (ε'') for (a) PP16, (b) PP18, (c) PP20, (d) PP22, (e) PP24, and (f) variation of conductivity and relaxation time with temperature for PP20.

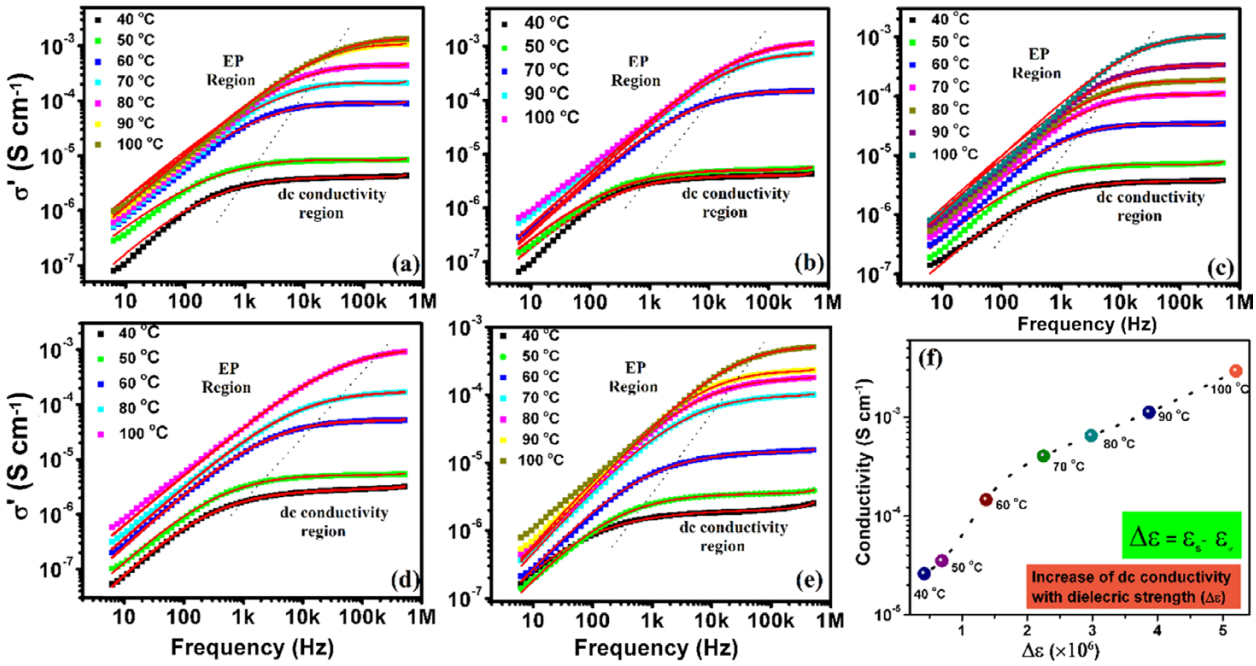

Figure 9. Frequency dependence of real part of complex conductivity (σ') for (a) PP16, (b) PP18, (c) PP20, (d) PP22, (e) PP24, and (f) variation of dielectric strength with temperature for PP20.

in low frequency associated with electrode polarization region due to slow reversal of field, (ii) frequency independent bulk dc conductivity region and high frequency dispersive region due to faster periodic reversal of field and hence the charge accumulation elimination lead to increase of the conductivity.[90,91] It is again interesting to notice here that with an increase of the temperature frequency dependent region associated with EP significantly increases. It indicates that the more ion accumulation participates in building up of polarization due to better salt dissociation which increases the number of free charge carriers. With the increase of temperature, dc conductivity regions decrease while dispersive regions following Jonscher power law disappear. It may be concluded that the EP phenomena, dc conductivity, and the dispersive region are correlated with each other with a strong dependency on the temperature.

The intermediate frequency plateau is used to extract the dc conductivity value by taking intercept at zero frequency and dc conductivity value increases with the temperature. At ambient temperature, the energy barrier is high due to coordination of the cation with host polymer and cation migration is linked with the polymer chain motion. At high temperature, increased polymer chain flexibility and rapid relaxation push the cation at a higher rate from one coordinating site to another, since anions are in the immobilized state to the polymer backbone. At high-temperature creation and destruction of the new favorable coordinating sites occurs speedily and the possibility of ion migration *via* hopping seems to be increased. The above concept is supported by the decreased value of relaxation time with the increase of the temperature. At hopping frequency, the transition from the dc conductivity to the dispersive region is observed.

The varying hopping distance due to thermal activation influence the cation migration *via* hopping. It is reported that with an increase of the temperature average hopping length ($\sqrt{\langle \lambda^2 \rangle}$) decreases. Another important parameter is hopping potential barrier (E_{hop}) that the ion must overcome a successful jump to the forthcoming coordination site. Now the average hopping length (distance between the neighboring ion pairs) decreases with the increase of temperature. The lowering of the hopping length leads to overlap of Coulomb potential wells and E_{hop} decreases which results in the improved mobility of ions hence the dc conductivity.[49,92] It is noted that the hopping frequency shifts toward the high-frequency window with an increase in the temperature. In brief, the probability of successful hopping for the cation increases that lead to the enhancement of the ionic conductivity which is also supported by lowering of relaxation time.[93] The solid line in the plot is best fit and it is worthy to note that both the experimental and simulated results are in good agreement in whole frequency window. Also, the experimental data reproduces the simulated data with an increase in the temperature.

Figure 9(f) shows the increase of the conductivity with an increase of the dielectric strength and temperature. The increase of dielectric strength indicates the increase of a number of free charge carriers which enhances the conductivity. The increase of dielectric strength with temperature is also linked with the better salt dissociation with an increase of temperature. Both the exponent α and n are almost independent of the temperature for all solid polymer electrolyte system. The value of α is almost close to 1 while the value of n lies between 0.46 and 0.52 with negligible dependency on the temperature.

3.6.2. Imaginary part of complex conductivity

Figure 10(a)-(e) shows the temperature dependent imaginary part of the complex conductivity (σ'') in the frequency range from 1 Hz to 1 MHz. The plot is divided into three regions, low frequency electrode polarization region, and an intermediate

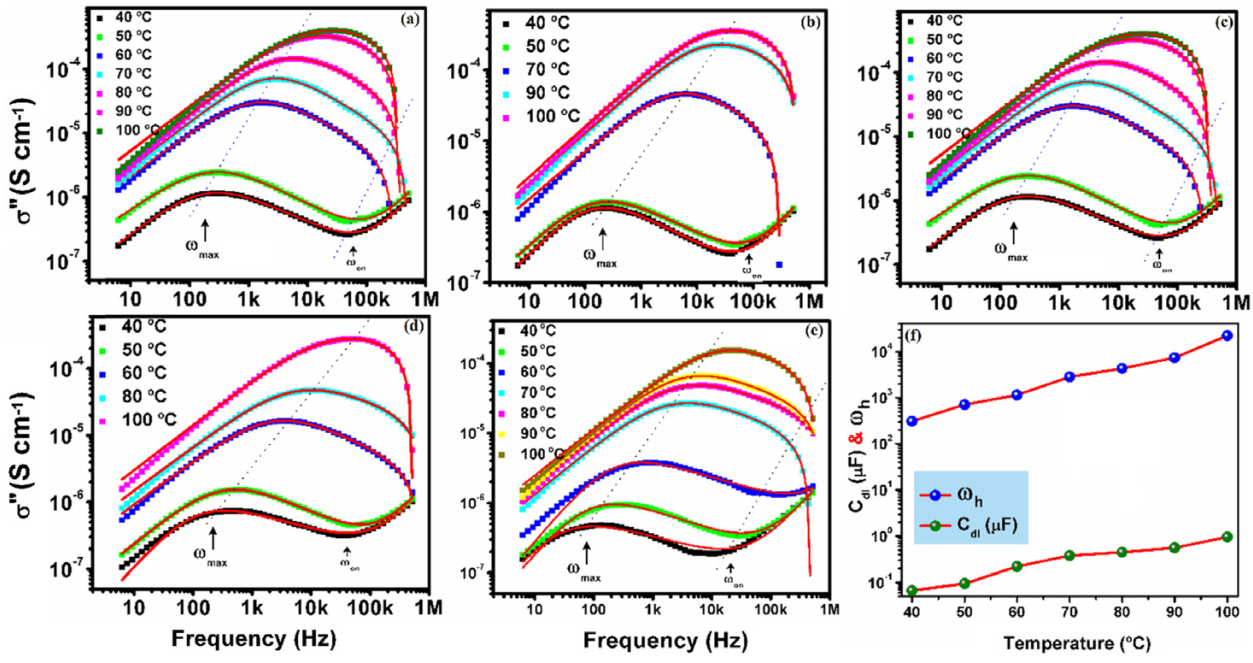

Figure 10. Frequency dependence of imaginary part of complex conductivity (σ'') for (a) PP16, (b) PP18, (c) PP20, (d) PP22, (e) PP24, and (f) variation of conductivity and relaxation time with temperature for PP20.

frequency region followed by the high frequency dispersion region. The investigated system shows the identical nature of the plot. Two peaks are obtained one for minimum σ'' at high frequency and another for maximum σ'' at low frequency.[49] The former peak is for ω_{on} is associated with the onset of the electrode polarization (EP) phenomena and continuously grow up to a frequency where σ'' shows maxima termed as ω_{max}. At this frequency maximum polarization is built up at electrode electrolyte interface.

Now, the temperature dependent imaginary part of the complex conductivity (σ'') is investigated. It may be observed that for all solid polymer electrolyte both ω_{on} and ω_{max} shift toward high frequency. Also, the EP window get broadened while the high frequency region depicting direct proportionality with frequency disappears with increase of temperature.[73] It may be concluded that the temperature plays an effective role in enhancing the conductivity and all systems are dependent on the temperature. Figure 10(f) shows the increase of the double layer capacitance and the hopping frequency with increase of the temperature that indicate the enhancement in the segmental motion of the polymer chain and lowering of relaxation time.

3.7. Correlation of hopping frequency and segmental motion of polymer chain

It has now been summarized that the ion migration in the investigated system is attributed to the charge carriers hopping linked with the segmental motion of the polymer chain. The enhanced amorphous content and faster segmental motion with temperature speed up the internal modes. So, the ion hopping at high frequency lead to enhancement of the ionic conductivity with reduction of average hopping length ($\sqrt{\langle \lambda^2 \rangle}$). To evidence, the correlation between the ion hopping and the segmental motion Debye-Stokes-Einstein plot was obtained as shown in Figure 11. The DSE equation is proposed for such system which shows weak dependency to temperature and is expressed as; $\sigma_{dc} \propto f_s \propto \omega_h$ (f_s is the segmental frequency).[87] The plot depicts the dc conductivity behavior according to the DSE equation for all SPE system with almost negligible deviation and evidence that the only free cation is contributing to conductivity with negligible contribution from the ion pairs. The enhancement of temperature promotes the diffusion of single lithium ions and is in agreement with the enhancement of the ionic conductivity.[94-96] In brief, it may be suggested that at particular frequency all systems depicts the coupling of the dc conductivity with the hopping frequency and only cation is playing the key role in the enhancement of ion dynamics.

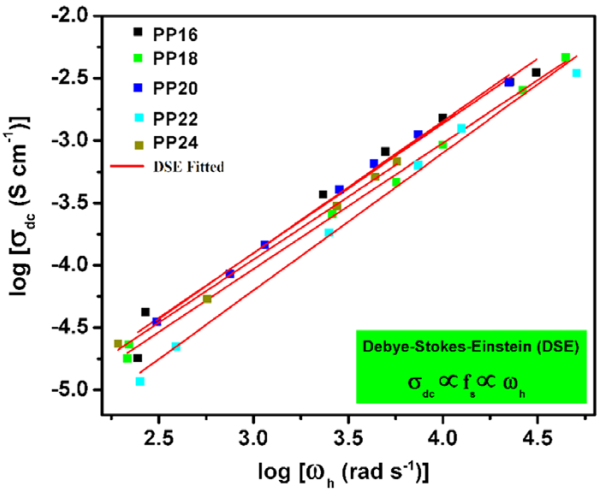

Figure 11. The plot of dc conductivity against the hopping frequency at different temperatures. Solid red lines are the best fit for the DSE equation.

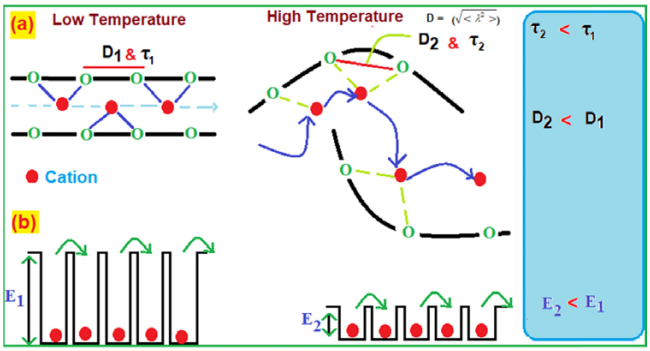

Figure 12. Temperature-dependent ion transport mechanism.

3.8. Ion transport mechanism

Now an interaction scheme based on the experimental results is proposed in two ways, (i) polymer segmental motion and (ii) hopping barrier. Initially when the polymer salt system shows a semi-rigid structure and ion migration occurs *via* the coordinating sites of the host polymer. As shown in Figure 12(a) that between two coordinating sites is specified hopping length (D_1) that is to be covered for a successful hopping (D_1) and relaxation time of the polymer chains is τ_1. So, when the temperature increases, then the system transform to the flexible system and hopping length of charge carriers decreases (D_2<D_1) owing to the availability of more coordinating sites easily (Figure 12(a)). Now, the faster relaxation of the polymer chain occurs as well as ion migration from one site to another is rapid as evidenced by the decrease of the relaxation time (τ_2<τ_1). The thermal activation of the charge carriers reduces the time spent by the cation at coordinating sites and faster ion dynamics is expected. The average time spent by the cation at a coordinating site decrease and ion diffusion become smoother.

The other important parameter is the hopping potential barrier (E_{hop}) which is the potential that must be overcome by the cation for successful hopping. Now when the temperature is lower then the hopping potential is indicated by the E_1 (Figure 12(b)). So, to jump from one site to forthcoming site ion must cross this barrier. Now, when the temperature increases then the average hopping length decreases. This lead to overlapping of the potential barriers and overall potential that must be overcome by the cation decreases denoted as E_2, as shown in Figure 12(b). The reduction in the potential barrier (E_2<E_1) suggest that the ion mobility is increased which directly indicates the enhancement of the ionic conductivity and the dielectric constant. In brief, it may be stated that the temperature plays an effective role in enhancing the dielectric properties and is a combination of the three mechanisms, (i) increase of the polymer flexibility, (ii) decrease in hopping length and, (iii) lowering of hopping potential barrier.

4. Conclusions

The lithium ion conducting blended solid polymer electrolyte matrix has been prepared through solution cast technique. The effect of the variation of salt content and temperature on the dielectric properties of prepared films has been investigated. The complex dielectric permittivity, loss tangent and complex conductivity were simulated and fitted results were in close agreement with the experimental findings. The increase in dielectric constant with salt content suggests the increase in a number of free ions due to better dissociation of salt and hence the conductivity. The tangent delta analysis reveals the shift of relaxation peak toward high frequency and lowering of the relaxation time with the addition of salt. The ac conductivity analysis is analyzed in the whole frequency window. The modulus formalism displays the increase of the capacitance with the addition of the salt. A fruitful correlation between the various relaxation times obtained from the fitting parameters is observed. The dielectric constant, ac conductivity & hopping frequency increases with temperature while, relaxation time decreases and simulated results are in absolute agreement with experimental results. The improvement in dielectric parameters may be due to faster ion migration *via* the segmental/slipping motion of polymer chain and the availability of more free charge carriers in the system. The dc conductivity, hopping frequency, and segmental motion are strongly coupled and cross-checked by the Debye-Stoke-Einstein (DSE) plot. A self-proposed mechanism has been developed to highlight the effect of temperature in enhancing the segmental motion and lowering the potential barrier of the investigated system.

References

(1) N. Nitta, F. Wu, J. T. Lee, and G. Yushin, *Mater. Today,* **18**, 252 (2015).
(2) V. Etacheri, R. Marom, R. Elazari, G. Salitra, and D. Aurbach, *Energy Environ. Sci.*, **4**, 3243 (2011).
(3) A. L. Sharma and A. K. Thakur, *J. Appl. Polym. Sci.*, **118**, 2743 (2010).
(4) M. S. Johnsi and S. A. Suthanthiraraj, *Macromol. Res.*, **26** 100 (2018).
(5) A. Arya and A. L. Sharma, *Ionics*, **23**, 497 (2017).
(6) W. Liu, N. Liu, J. Sun, P. C. Hsu, Y. Li, H. W. Lee, and Y. Cui, *Nano Lett.*, **15**, 2740 (2015).
(7) J. Mindemark, M. J. Lacey, T. Bowden, and D. Brandell, *Prog. Polym. Sci.*, **81**, 114 (2018).
(8) J. Zheng, Y. Y. Hu, *ACS Appl. Mater. Interfaces*, **10**, 4113 (2018).
(9) J. B. Goodenough and P. Singh, *J. Electrochem. Soc.,* **162**, 2387 (2015).
(10) A. L. Sharma and A. K. Thakur, *Ionics*, **19**, 795 (2013).
(11) A. Arya and A. L. Sharma, *J. Phys. D: Appl. Phys.*, **51**, 045504 (2018).
(12) L. Long, S. Wang, M. Xiao, and Y. Meng, *J. Mater. Chem. A*, **4** 10038 (2016).
(13) J. Yi, S. Guo, P. He, and H. Zhou, *Energy Environm. Sci.,* **10** 860 (2017).
(14) C. M. Costa, M. M. Silva, and S. Lanceros-Méndez, *RSC Adv.*, **3**, 11404 (2013).
(15) C. Bhatt, R. Swaroop, A. Arya, and A. L. Sharma, *J. Mater. Sci. Eng. B*, **5**, 418 (2015).
(16) D. Fragiadakis, S. Dou, R. H. Colby, and J. Runt, *Macromolecules*, **41**, 5723 (2008).
(17) S. J. Park, A. R. Han, J. S. Shin, and S. Kim, *Macromol. Res.*, **18**, 336 (2010)
(18) A. Arya and A. L. Sharma, *Appl. Sci. Lett.,* **2**, 72 (2016).
(19) A. Arya, M. Sadiq, and A. L. Sharma, *Ionics*, **24**, 2295 (2018).
(20) A. M. Rocco, R. P. Pereira, and M. I. Felisberti, *Polymer*, **42**, 5199 (2001).
(21) K. M. Anilkumar, B. Jinisha, M. Manoj, and S. Jayalekshmi, *Eur. Polym. J.,* **89**, 249 (2017).
(22) E. M. Abdelrazek, I. S. Elashmawi, A. El-Khodary, and A. Yassin, *Curr. Appl. Phys.*, **10**, 607 (2010).

(23) A. Arya and A. L. Sharma, *J. Solid State Electrochem.*, **22**, 2725 (2018).
(24) B. K. Choi, Y. W. Kim, and H. K. Shin, *Electrochim. Acta*, **45**, 1371 (2000).
(25) M. M. Jacob, S. R. Prabaharan, and S. Radhakrishna, *Solid State Ionics,* **104**, 267 (1997).
(26) A. Arya, S. Sharma, A. L. Sharma, D. Kumar, and M. Sadiq, *Asian J. Eng. Appl. Technol.,* **5**, 4 (2016).
(27) L. Fan, Z. Dang, C. W. Nan, and M. Li, *Electrochim. Acta*, **48**, 205 (2002).
(28) P. Joge, D. K. Kanchan, P. Sharma, and N. Gondaliya, *Indian J. Pure Appl. Phys.,* **51**, 350 (2013).
(29) T. M. Ali, N. Padmanathan, and S. Selladurai, *Ionics*, **21**, 829 (2015).
(30) M. Premalatha, N. Vijaya, S. Selvasekarapandian, and S. Selvalakshmi, *Ionics*, **22**, 1299 (2016).
(31) R. L. Thankamony, H. Chu, S. Lim, T. Yim, Y. J. Kim, T. H. Kim, *Macromol. Res.*, **23**, 38 (2015).
(32) A. Arya and A. L. Sharma, *J. Phys. D: Appl. Phys.*, **50**, 443002 (2017).
(33) K. Karuppasamy, R. Antony, S. Alwin, S. Balakumar, and X. Sahaya Shajan, *Mater. Sci. Forum*, **807**, 41 (2015).
(34) A. R. Polu, R. Kumar, and H. W. Rhee, *Ionics,* **21**, 125 (2015).
(35) K. K. Kumar, M. Ravi, Y. Pavani, S. Bhavani, A. K. Sharma, V. N. Rao, *Physica B: Condens. Matter*, **406**, 1706 (2011).
(36) K. Xu, S. Zhang, T. R. Jow, W. Xu, and C. A. Angell, *Electrochem. Solid-State Lett.,* **5**, 26 (2002).
(37) L. F. Li, B. Xie, H. S. Lee, H. Li, X. Q. Yang, J. McBreen, and X. J. Huang, *J. Power Sources*, **189**, 539 (2009).
(38) F. I. Chowdhury, M. U. Khandaker, Y. M. Amin, M. Z. Kufian, and H. J. Woo, *Ionics*, **23**, 275 (2017).
(39) I. S. Noor, S. R. Majid, and A. K. Arof, *Electrochim. Acta*, **102**, 149 (2013).
(40) G. B. Appetecchi, D. Zane, and B. Scrosati, *J. Electrochem. Soc.*, **151**, 1369 (2004).
(41) R. J. Sengwa and S. Choudhary, *J. Alloys Compd.*, **701**, 652 (2017).
(42) S. Choudhary and R. J. Sengwa, *J. Appl. Polym. Sci.*, **132**, 41311 (2015).
(43) S. Das and A. Ghosh, *J. Phys. Chem. B,* **121**, 5422 (2017).
(44) S. Choudhary and R. J. Sengwa, *Mater. Chem. Phys.,* **142**, 172 (2013).
(45) R. J. Sengwa and S. Choudhary, *Express Polym. Lett.*, **4**, 559 (2010).
(46) A. Arya and A. L. Sharma, *J. Phys. Condens. Matter*, **30**, 165402 (2018).
(47) K. S. Cole and R. H. Cole, *J. Chem. Phys.*, **9**, 341 (1941).
(48) R. M. Hill and A. K. Jonscher, *Contemp. Phys.*, **24**, 75 (1983).
(49) A. Roy, B. Dutta, and S. Bhattacharya, *RSC Adv.,* **6**, 65434 (2016).
(50) U. H. Choi and B. M. Jung, *Macromol. Res.*, **26**, 459 (2018).
(51) A. Arya and A. L. Sharma, *J. Mater. Sci. Mater. Electron.*, **29**, 17903 (2018).
(52) P. Y. Yamada, D. Daneshvari, R. Pittini, S. Vaucher, L. Rohr, S. Leparoux, and H. Leuenberger, *Eur. Polym. J.,* **44**, 1191 (2008).
(53) G. Hu, F. Gao, J. Kong, S. Yang, Q. Zhang, Z. Liu, and H. Sun, *J. Alloys Compd.*, **619**, 686 (2015).
(54) H. J. Woo, S. R. Majid, and A. K. Arof, *Solid State Ionics,* **199**, 14 (2011).
(55) C. S. Prasanna and S. A. Suthanthiraraj, *Ionics*, **24**, 2631 (2018).
(56) A. G. L. A. I. A. Vassilikou-Dova, and I. M. Kalogeras, in *Thermal Analysis of Polymers: Fundamentals and Applications*, John Wiley, Hoboken, New Jersey, 2009, pp 497-613.
(57) A. L. Sharma and A. K. Thakur, *Ionics*, **17**, 135 (2011).
(58) K. S. Ngai, S. Ramesh, K. Ramesh, and J. C. Juan, *Chem. Phys. Lett.*, **692**, 19 (2018).
(59) A. Awadhia, S. K. Patel, and S. L. Agrawal, *Prog. Cryst. Growth Charact. Mater.*, **52**, 61 (2006).
(60) M. Sadiq, A. Arya, and A. L. Sharma, *Springer Proc. Phys.,* **178**, 389 (2017).
(61) H. J. Woo, S. R. Majid, and A. K. Arof, *Mater. Chem. Phys.,* **134**, 755 (2012).
(62) P. Bose, A. Roy, B. Dutta, and S. Bhattacharya, *Solid State Ionics*, **311**, 75 (2017).
(63) M. Ravi, Y. Pavani, K. Kiran Kumar, S. Bhavani, A. K. Sharma, and V. V. R. Narasimha Rao, *Mater. Chem. Phys.*, **130**, 442 (2011).
(64) S. Chopra, S. Sharma, T. C. Goel, and R. G. Mendiratta, *Solid State Commun.*, **127**, 299 (2003).
(65) A. L. Sharma and A. K. Thakur, *Ionics*, **21**, 1561 (2015).
(66) A. K. Arof, S. Amirudin, S. Z. Yusof, and I. M. Noor, *Phys. Chem. Chem. Phys.*, **16**, 1856 (1856)
(67) K. Nakamura, T. Saiwaki and K. Fukao, *Macromolecules,* **43**, 6092 (2010).
(68) P. Pal and A. Ghosh, *J. Appl. Phys.*, **120**, 045108 (2016).
(69) A. Roy, B Dutta, and S. Bhattacharya, *Ionics*, **23**, 3389 (2017).
(70) K. Funke, *Solid State Ionics,* **94**, 27 (1997).
(71) J. C. Dyre, *J. Appl. Phys.*, **64**, 2456 (1988).
(72) P. S. Anantha and K. Hariharan, *Mater. Sci. Eng. B*, **121**, 12 (2005).
(73) I. Fuentes, A. Andrio, F. Teixidor, C. Vinas, and V. Compan, *Phys. Chem. Chem. Phys.*, **19**, 15177 (2017).
(74) I. Popov, P. B. Ishai, A. Khamzin, and Y. Feldman, *Phys. Chem. Chem. Phys.*, **18**, 13941 (2016).
(75) M. C. R. Shastry and K. J. Rao, *Solid State Ionics*, **44**, 187 (1991).
(76) S. Austin Suthanthiraraj, D. Joice Sheeba, and B. Joseph Paul, *Mater. Res. Bull.,* **44**, 1534 (2009).
(77) R. J. Sengwa, S. Choudhary, and S. Sankhla, *Express Polym. Lett.,* **2**, 800 (2008).
(78) A. L. Sharma and A. K. Thakur, *J. Mater. Sci.*, **46**, 1916 (2011).
(79) F. S. Howell, R. A. Bose, P. B. Macedo, and C. T. Moynihan, *J. Phys. Chem.,* **78**, 639 (1974).
(80) S. Choudhary and R. J. Sengwa, *Electrochim. Acta*, **247**, 924 (2017).
(81) H. M. Ng, S. Ramesh, and K. Ramesh, *Org. Electron.,* **22**, 132 (2015).
(82) H. E. Atyia and N. A. Hegab, *Optik*, **127**, 6232 (2016).
(83) Z. M. Dang, J. K. Yuan, S. H. Yao, and R. J. Liao, *Adv. Mater.*, **25**, 6334 (2013).
(84) I. M. Hodge, M. D. Ingram, and A. R. West, *J. Electroanal. Chem. Interfacial Electrochem.,* **74**, 125 (1976).
(85) J. Mal and R. N. P. Choudhary, *Phase Transitions*, **62**, 119 (1997).
(86) P. B. Bhargav, V. M. Mohan, A. K. Sharma, and V. N. Rao, *Curr. Appl. Phys.*, **9**, 165 (2009).
(87) D. Fragiadakis, S. Dou, R. H. Colby, and J. Runt, *J. Chem. Phys.*, **130**, 064907 (2009).
(88) G. Govindaraj, N. Baskaran, K. Shahi, and P. Monoravi, *Solid State Ionics*, **76**, 47 (1995).
(89) A. S. Nowick and B. S. Lim, *J. Non-Cryst. Solids*, **172**, 1389 (1994).
(90) S. Ramesh, C. W. Liew, and A. K. Arof, *J. Non-Cryst. Solids*, **357**, 3654 (2011).
(91) N. Chilaka and S. Ghosh, *Electrochim. Acta*, **134**, 232 (2014).
(92) P. G. Bruce and F. M. Gray, *Solid State Electrochemistry*. Cambridge University Press, Cambridge, 1995.
(93) T. Dam, S. S. Jena, and D. K. Pradhan, *Phys. Chem. Chem. Phys.*, **18**, 19955 (2016).
(94) N. H. LaFemina, Q. Chen, R. H. Colby, and K. T. Mueller, *J. Chem. Phys.*, **145**, 114903 (2016).
(95) R. Rathika and S. A. Suthanthiraraj, *Macromol. Res.*, **24**, 422 (2016).
(96) J. Yu, W. Wu, D. Dai, Y. Song, C. Li, and N. Jiang, *Macromol. Res.*, **22**, 19 (2014).